ACS Catalysis

pubs.acs.org/acscatalysis Research Article

Unprecedented Catalysis of Cs^+ Single Sites Confined in Y Zeolite Pores for Selective C_{sp3}–H Bond Ammoxidation: Transformation of Inactive Cs^+ Ions with a Noble Gas Electronic Structure to Active Cs^+ Single Sites

Shankha S. Acharyya,[‖] Shilpi Ghosh,[‖] Yusuke Yoshida, Takuma Kaneko, Takehiko Sasaki,*[,‖] and Yasuhiro Iwasawa*[,‖]

Cite This: *ACS Catal.* 2021, 11, 6698–6708 Read Online

ACCESS | Metrics & More | Article Recommendations | Supporting Information

ABSTRACT: We report the transformation of Cs^+ ions with an inactive noble gas electronic structure to active Cs^+ single sites chemically confined in Y zeolite pores (Cs^+/Y), which provides an unprecedented catalysis for oxidative cyanation (ammoxidation) of C_{sp3}–H bonds with O_2 and NH_3, although in general, alkali and alkaline earth metal ions without a moderate redox property cannot activate C_{sp3}–H bonds. The Cs^+/Y catalyst was proved to be highly efficient in the synthesis of aromatic nitriles with yields >90% in the selective ammoxidation of toluene and its derivatives as test reactions. The mechanisms for the genesis of active Cs^+ single sites and the ammoxidation pathway of C_{sp3}–H bonds were rationalized by density functional theory (DFT) simulations. The chemical confinement of large-sized Cs^+ ions with the pore architecture of a Y zeolite supercage rendered the highest occupied molecular orbital (HOMO)–lowest unoccupied molecular orbital (LUMO) gap reduction, HOMO component change, and preferable coordination arrangement for the selective reaction promotion, which provides a trimolecular assembly platform to enable the coordination-promoted concerted ammoxidation pathway working closely on each Cs^+ single site. The new reaction pathway without involvement of O_2-dissociated O atom and lattice oxygen differs from the traditional redox catalysis mechanisms for the selective ammoxidation.

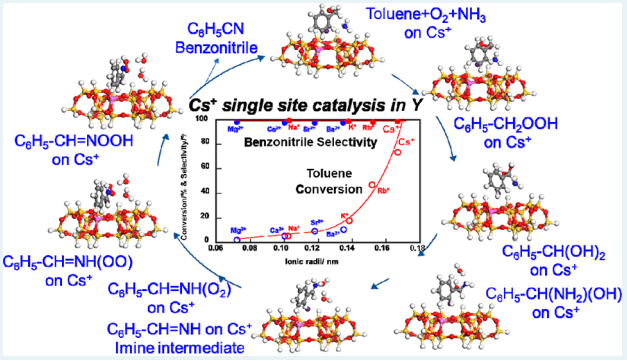

KEYWORDS: *catalytic C_{sp3}–H activation, confined Cs^+ single site in Y zeolite pore, ammoxidation of toluene and its derivatives, selective nitrile synthesis, catalysis mechanism*

1. INTRODUCTION

Alkali metal ions with inactive noble gas electronic structures have been conceived as inactive species for selective functionalization of C_{sp2}–H and C_{sp3}–H bonds to useful chemicals in industry. Recently, we found a single alkali metal ion site platform in a β zeolite pore that selectively promoted benzene C_{sp2}–H activation toward phenol synthesis.[1,2] The catalytic performance of alkali metal ion sites incorporated in zeolite pores depended strongly on the kind of zeolites, and ZSM-5, mordenite, and Y zeolites were almost inactive as supports. No C_{sp3}–H activation catalysis of alkali metal ions and oxides has been achieved to date, although a variety of effects of alkali metal additives on metal oxide catalysis are known.[3] Here, we report the first example of the catalytic selective activation of C_{sp3}–H bonds to produce C–N bonds on Cs^+ single ion sites in Y zeolite pores (Cs^+/Y) due to transformation of inactive Cs^+ ions with a noble gas electronic structure to active Cs^+ sites with HOMO(O 2p)–LUMO(Cs 6s) by chemical confinement of Cs^+ ions at Y zeolite pore surfaces, making Cs–O bonds and reactive coordination. Ammoxidation of methyl C_{sp3}–H bonds of aromatics with O_2 + NH_3 is an avenue for the synthesis of organic nitriles, which have been commercially used as common building blocks for high-performance rubbers, polymers, and molecular electronics and also as integral parts for producing pharmaceuticals, agrochemicals, and fine chemicals, such as vitamins, heterocycles, and various carboxylic acid derivatives.[4,5] Generally, organic nitriles were synthesized by cyanation of aldehydes using toxic hydrogen cyanide and metal cyanides, which caused environmental disasters.[3,6−9] Industrially, the vapor-phase

Received: February 28, 2021
Revised: April 26, 2021
Published: May 24, 2021

https://doi.org/10.1021/acscatal.1c00946
ACS Catal. 2021, 11, 6698–6708

Table 1. Catalytic Performances of Various Alkali and Alkaline Earth Metal Ion Single Sites in Different Zeolite Pores and Hydrotalcite Interlayers and on a SiO_2·Al_2O_3 Surface for the Toluene Ammoxidation to Benzonitrile (PhCN) at 623 K[a,b]

entry	catalyst	toluene conv./%	PhCN selec./%	PhCN syn. rate/μmol s^{-1} g^{-1}_{cat}	NH_3/PhCN
1	Y zeolite	0		0	
2	Mg^{2+}(2 wt %)/Y	2.2	97.8	0.017	18.1
3	Ca^{2+}(2 wt %)/Y	5.1	97.5	0.04	19.4
4	Sr^{2+}(2 wt %)/Y	9.0	97.0	0.08	10.0
5	Ba^{2+}(2 wt %)/Y	11.2	97.5	0.09	14.6
6	Na^{+}(2 wt %)/Y	4.9	98.9	0.04	2.8
7	K^{+}(2 wt %)/Y	17.6	98.5	0.14	2.1
8	Rb^{+}(2 wt %)/Y	47.1	98.1	0.40	1.2
9	Cs^{+}(2 wt %)/Y	77.1	98.5	0.60	1.0
10	Cs^{+}(2 wt %)/β	31.3	97.3	0.23	2.1
11	Cs^{+}(2 wt %)/ZSM-5	1.0	79.3	0.006	173
12	Cs^{+}(2 wt %)/Mor	1.0	86.1	0.006	411
13	Cs^{+}(2 wt %)/Hydr	0.2	0	0	
14	Cs^{+}(2 wt %)/$SiAlO_x$	0.03	0	0	
15	Cs^{+}(2 wt %)/Y[c]	34.8	98.9	0.27	2.0
16	Cs^{+}(2 wt %)/Y[d]	93.7	96.6	0.71	5.0
17	Cs^{+}(2 wt %)/Y[e]	94.6	98.0	0.36	1.3
18	Cs^{+}(2 wt %)/Y[f]	0		0	
19	Cs^{+}(2 wt %)/Y[g]	0		0	
20	Cs^{+}(2 wt %)/Y[h]	0[i]			

[a]Y = Y zeolite with SiO_2/Al_2O_3 molar ratio of 30, purchased from Zeolyst Co. Conv. = conversion; selec. = selectivity; NH_3/PhCN = molar ratios of consumed NH_3 to synthesized PhCN; zeolites = Y, β, ZSM-5, and mordenite (Mor); Hydr = hydrotalcite; $SiAlO_x$ = SiO_2·Al_2O_3 with the same SiO_2/Al_2O_3 molar ratio (30) as the Y zeolite. Performance values were averaged during 30−240 min time-on-stream. [b]Reaction conditions: toluene/O_2/NH_3/He = 0.20/1.0/1.8/5.0 (mL min^{-1}); cat. = 0.2 g. [c]Reaction conditions: 603 K. [d]Reaction conditions: 673 K. [e]Reaction conditions: 0.4 g, 623 K. [f]Reaction conditions: toluene + O_2; toluene/O_2/He = 0.20/1.0/5.0 (mL min^{-1}). [g]Reaction conditions: toluene + NH_3; toluene/NH_3/He = 0.20/1.8/5.0 (mL min^{-1}). [h]Reaction conditions: O_2 + NH_3; O_2/NH_3/He = 1.0/1.8/5.0 (mL min^{-1}). [i]NH_3 conversion/%.

ammoxidation of toluene to benzonitrile has been extensively studied with metal and metal oxide catalysts of V, Cr, Mo, etc.,[10−25] whose catalysts possess moderate redox potentials and sufficient M−O bond strengths to provide active lattice oxygen and oxygen atoms at the catalyst surfaces for the redox catalysis. The Cs^+/Y catalyst without a beneficial redox property showed a high benzonitrile yield (92.7% yield; 94.6% conversion and 98.0% selectivity at 623 K) and a high NH_3 utilization efficiency (almost no extra consumption) in toluene ammoxidation employed as a test reaction; to the best of our knowledge, this is the highest yield without NH_3 loss for the benzonitrile synthesis from toluene with O_2 + NH_3 in a single-step gas-phase reaction. There is always a competition between the ammoxidation to benzonitrile and undesirable NH_3 oxidation to N_2 and NO_x on catalyst surfaces,[1−3,11,23] whereas the Cs^+/Y was found to catalyze no NH_3 + O_2 reaction when toluene was not present (Table 1). The simple ion-exchange method for the chemically confined Cs^+/Y catalyst fabrication in this study is also advantageous in industrial usage. The Cs^+/Y catalyst was also effective in the synthesis of other organic nitriles, thereby proving its versatility. The genesis and mechanism of the unprecedented catalysis by the Cs^+ single ion site/Y, which differs from the traditional redox catalysis mechanisms, has been characterized by X-ray photoelectron spectroscopy (XPS), scanning transmission electron microscopy−energy-dispersive X-ray spectroscopy (STEM-EDS), X-ray diffraction (XRD), temperature-programmed desorption (TPD), in situ X-ray absorption near-edge structure (XANES) and extended X-ray absorption fine structure (EXAFS), and DFT calculations.

2. EXPERIMENTAL SECTION

2.1. Catalyst Synthesis. Zeolite Y-supported alkali metal ion and alkaline earth metal ion catalysts were prepared by a reliable ion-exchange method,[1,2] followed by a controlled treatment at 573 K, using the corresponding metal nitrates as precursors. A typical Cs^+(2 wt %)/Y sample was synthesized as follows. $CsNO_3$ (0.88 g) (Kanto Chemical Co.) was dissolved in 10 mL of deionized water in a 50 mL Erlenmeyer flask, to which 2.91 g of NH_4−Y with SiO_2/Al_2O_3 = 30 (purchased from Zeolyst Co.) was added with stirring. For the ion-exchange of NH_4^+ ions with Cs^+ ions, the solution was heated from room temperature to 353 K and maintained at 353 K for 12 h with stirring, followed by washing with deionized water, centrifuging, and finally drying at 353 K for 8 h. Other zeolite Y-supported alkali and alkaline earth metal ion catalysts were prepared similarly. Cs^+(2 wt %)/Y samples with different SiO_2/Al_2O_3 ratios (5.2, 5.6, 12, and 115) were also prepared in a similar way. Furthermore, other supports for Cs^+ (β, ZSM-5, mordenite (Mor), hydrotalcite (Hydr), and silica−alumina (SiO_2·Al_2O_3)) were also used to prepare different supported Cs^+ catalysts for comparison.

2.2. Catalytic Reactions and Product Analysis. Vapor-phase ammoxidation of toluene was carried out at atmospheric pressure using a fixed-bed flow reactor (Pyrex glass tube) with an inner diameter of 6 mm and externally heated by electric resistances. The reaction temperature was measured inside the catalyst bed by a thermocouple, whose tip was placed inside the upper side of the catalyst bed. Catalyst powders were pressed to pellets, crushed, and sieved (typically, 0.2 g, sieved into 500−850 μm particles), and the sieved samples were packed between quartz wool in the flow reactor. Toluene was fed continuously into the gas stream by using a syringe pump.

https://doi.org/10.1021/acscatal.1c00946
ACS Catal. 2021, 11, 6698−6708

The reactor was fed with a toluene/NH_3/O_2/He mixture in the molar ratio of 0.20/1.8/1.0/5.0 mL min^{-1} typically. The flow ratio of NH_3 to toluene was deliberately kept ~9 times larger in order to increase the nitrile selectivity because the formation of CO_2 decreases considerably with increasing amounts of NH_3 in the feed. The conversion and selectivity in the current system were calculated by using NH_3 as an internal standard, taking into account the calibration factors for NH_3 in the flame ionization detector (FID) and thermal conductivity detector (TCD) GCs in a similar way to that in our previous reports, assuming no loss of nitrogen in the material balance during the catalytic reactions.[1] The outlet stream was sampled with six-way sampling valves heated at 463 K using an online Shimadzu GC-2014 with a FID using a ZB-WAX plus capillary column (30 m, Phenomenex CA) for NH_3, tolue,ne and benzonitrile and a Shimadzu GC-2014 with a TCD using a WG-100 column (GL Science Japan) for O_2, N_2, CO, CO_2, NH_3, and H_2O. Helium was used as the carrier gas. The column temperature for TCD was 323 K. The column temperature for FID was held at 413 K for the first 2 min and then increased to 473 K at a heating rate of 298 K min^{-1}. For the ammoxidation of toluene in the present system, the nitrogen-containing products were N_2 and benzonitrile (PhCN) with a negligible amount of $PhCONH_2$. GC-TCD analysis showed no formation of N_2O. The values of the elemental carbon and nitrogen mass balances were estimated to be between 97% and 100% in most of the experimental runs.

2.3. Temperature-Programmed Desorption. All temperature-programmed desorption (TPD) experiments were carried out in a flow reaction system in a flow of helium carrier gas (50 mL min^{-1}). For each experiment in a fixed-bed reactor (6 mm i.d.), 0.2 g of catalysts with similar grain sizes (0.2−0.4 mm) were used. The catalysts were heated under He flow (4 mL min^{-1}) at 573 K for 30 min and cooled down to adsorption temperature (300 K). Respective flows of CO_2 and CH_3CN were turned on at 5 mL min^{-1} and kept for 15 min to complete their adsorption. The samples after the adsorption were flushed with helium (40 mL min^{-1}) for 15 min and then heated at a ramping rate of 28.3 K min^{-1}. The analysis of reactor effluents (CO_2 and CH_3CN) was performed on gas chromatographs with a thermal conductivity detector (TCD) and a flame ionization detector (FID), respectively, calibrated by the peak area of known pulses of the respective chemicals. NH_3 TPD experiments on Cs^+(2 wt %)/Y and Cs^+(2 wt %)/β at 353−923 K were also conducted in a similar way to the earlier TPD experiments to examine the adsorption behavior and strength of NH_3 in relation to the ammoxidation catalysis mechanism.

2.4. In Situ X-ray Absorption Fine Structure Measurements and Data Analysis. In situ X-ray absorption fine structure (XAFS) spectra at the Cs L_3-edge for the as-synthesized Cs^+(2 wt %)/Y sample and after the pretreatment and catalysis of the sample without exposure to air were measured at 15 K in a fluorescence mode at a BL36XU station in SPring-8. XANES and EXAFS spectra were analyzed in a similar way to that in previous reports,[1,26] using the Larch code containing the IFEFFIT Package ver. 2 (Athena and Artemis).[27] Background subtraction in the EXAFS analysis was performed using Autobk.[28] The Victoreen function was employed for the background subtraction, and the spline smoothing method with Cook and Sayers criteria was used as the μ_0 method. The extracted k^2-weighted EXAFS oscillations were Fourier-transformed to R-space over k = 25−80 nm^{-1}, and the curve fittings were performed in the R-space (0.18−0.32 nm). The fitting parameters for each shell were coordination number (CN), interatomic distance (R), Debye−Waller factor (σ^2), and correction-of-edge energy (ΔE_0). The phase shifts and amplitude functions for Cs−O and Cs−Cs were calculated from the FEFF 8.4 code.[29] Error ranges of the curve-fitting analysis of EXAFS Fourier transforms were based on the definition of the Larch code.[27]

2.5. DFT Calculations. All calculations were conducted with Dmol3 ver. 2018 (Biovia) on Materials Studio 2018.[30,31] A numerical basis set with polarization function (DNP), of which quality is comparable to 6-31G*, was adopted. All electrons were explicitly included. All possible multiplicities of electronic states were compared in the calculations, and optimized multiplicity was determined in each system. The Perdew−Wang 91 functional (PW91)[32] was used in all of the calculations. Transition states were searched by Dmol3 with the complete quadratic synchronous transit (QST)/linear synchronous transit (LST) option, where the LST maximization was performed for the coordinates interpolated between a reactant and a product, followed by repeated conjugated gradient minimizations and the QST maximizations until a transition state was located.[33,34]

To include the HY (Faujasite: FAU) zeolite framework, a cluster containing a 6-membered ring with 12 neighboring 4-membered rings was taken from the crystal structure of the FAU zeolite with hydrogen atom termination (Si−H). One Si atom in the 6-memebered ring was replaced by an Al atom by adding a H atom on the neighboring oxygen atom. Positions of the Al atom, the added H atom, and neighboring oxygen atoms were relaxed in the structural optimization. Then the H atom was replaced by a Cs atom, and the positions of the Cs atom, the Al atom, and neighboring O atoms were relaxed. The model ($Cs_1Si_{23}Al_1O_{37}H_{23}$) obtained in this way was used to examine the adsorption of toluene, O_2, NH_3, and subsequent intermediates and transition states. Plots for densities of state were drawn with respect to the Fermi level corresponding to the midpoint between HOMO and LUMO as the origin.

3. RESULTS AND DISCUSSION

3.1. Catalytic Performances of Cs^+/Y and Other Supported Alkali and Alkaline Earth Metal Ions. We have examined catalytic performances of alkali and alkaline earth metal ions, which were chemically confined in various zeolite pores and hydrotalcite interlayers and supported on a SiO_2·Al_2O_3 surface, in gas-phase ammoxidation (oxidative cyanation) of toluene with O_2 and NH_3 on 0.2 g of catalysts at 623 K as a test reaction. The results are shown in Table 1. Alkaline earth metal ions (Mg^{2+}, Ca^{2+}, Sr^{2+}, Ba^{2+})/Y samples (Y zeolite: SiO_2/Al_2O_3 molar ratio = 30) were incapable of activating C_{sp3}−H bonds as expected, and alkali metal ions (Na^+ and K^+)/Y samples also showed insufficient activity for benzonitrile (PhCN) synthesis, whereas Rb^+/Y and particularly Cs^+/Y possessed great potential to functionalize a toluene C_{sp3}−H bond toward PhCN. The toluene conversions were 47.1% and 73.0%, respectively, and the PhCN selectivities were as high as 98.1% and 98.5%, respectively; the only byproduct was CO_2, and no other liquid byproducts were observed. It is noteworthy that the Rb^+/Y and Cs^+/Y catalysis showed a remarkable suppression of undesirable NH_3 oxidation to N_2 and NO_x; the ratios of NH_3(consumed)/PhCN(synthesized) were 1.2 and 1.0, respectively, which are

https://doi.org/10.1021/acscatal.1c00946
ACS Catal. 2021, 11, 6698−6708

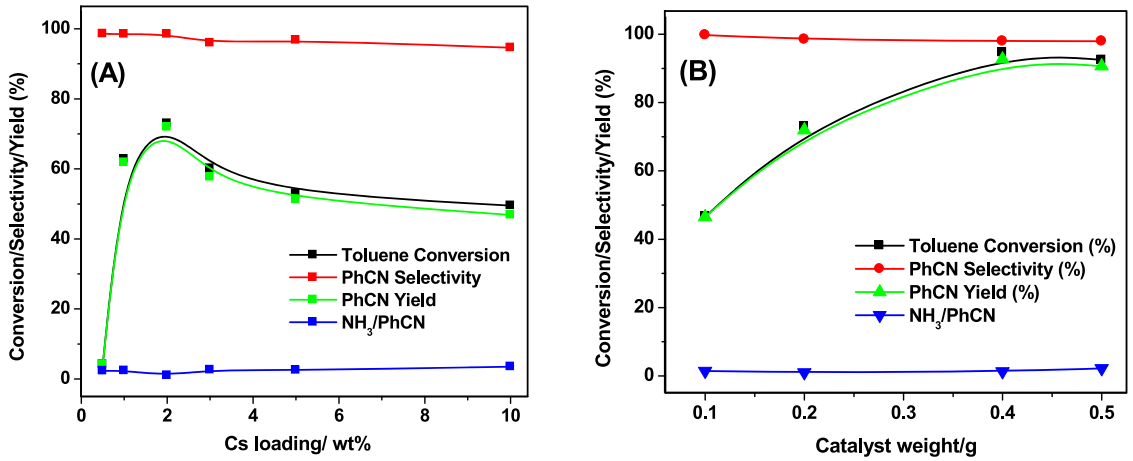

Figure 1. Catalytic activity of Cs^+/Y vs Cs loading (0.2 g of cat) (A) and catalyst weight (B).

nearly stoichiometric in the ammoxidation reaction equation, $C_6H_5CH_3 + 3/2O_2 + NH_3 \rightarrow C_6H_5CN$ (PhCN) $+ 3H_2O$.

To examine the influence of zeolite compositions (SiO_2/Al_2O_3 molar ratios) on the Cs^+/Y catalysis, toluene ammoxidation on Cs^+(2 wt %)/Y samples with different Si/Al ratios was performed. The results are shown in Table S1 (Supporting Information). It was observed that the Cs^+(2 wt %)/Y with SiO_2/Al_2O_3 = 12 showed a similar selectivity of 94.8−98.0% for the Cs^+(2 wt %)/Y with SiO_2/Al_2O_3 = 30 while keeping a high toluene conversion (98.5%), but undesired extra NH_3 oxidation to N_2 became about double under the reaction conditions in Table S1. By decreasing the SiO_2/Al_2O_3 ratio to 5.2−5.6, the selectivity toward benzonitrile decreased to 80.0−81.3% at 97.2−93.1% conversion, which indicates that strong Brønsted acidic sites in the Y zeolite promote the formation of undesired products (mainly CO_2) and undesired NH_3 oxidation. When the SiO_2/Al_2O_3 ratio was as high as 115, the toluene conversion abruptly decreased to 14.2% (Table S1), indicating the necessity of sufficient proton sites for ion-exchange with Cs^+ ions favorably near surface layers of zeolite particles. Among the samples examined in this study, Cs^+(2 wt %)/Y with SiO_2/Al_2O_3 molar ratio = 30 proved to be superior.

The performance (PhCN yield) of Cs^+/β was 40% of that of Cs^+/Y, as shown in Table 1. Other zeolites such as ZSM-5 and mordenite (Mor) were not effective as support for Cs^+ (0.79% and 0.86% yields, respectively; Table 1). Cs^+/hydrotalcite (Hydr), where Cs^+ ions are located in the interlayers of hydrotalcite, showed no activity for the ammoxidation. $Cs^+/SiO_2{\cdot}Al_2O_3$ with the same SiO_2/Al_2O_3 molar ratio (30) as the Y zeolite, where Cs^+ ions were supported on the $SiO_2{\cdot}Al_2O_3$ surface, was inactive (Table 1). These results suggest the importance of the pore architecture of the Y zeolite to confine Cs^+ chemically at the pore surface; thereby inactive Cs^+ ions with a noble gas electronic structure were transformed to active Cs^+ ion sites. The effect of Cs loading in 0.2 g of Cs^+/Y on the catalytic performance at 623 K was examined in the Cs loading range of 0.5−10.0 wt % as shown in Figure 1 and Table S2. The activity of the Cs^+ ions varied with the amount of Cs^+ ions in the Y zeolite. The conversion and selectivity gradually decreased to a saturated level after a maximum at 2.0 wt % Cs loading. The decrement of the catalytic activity of Cs^+/Y catalysts with increasing Cs loadings above 2.0 wt % may be attributed to the decreasing accessibility of Cs^+ sites at deeper layers of zeolite particles. At the moment we cannot discuss in more detail on the influence of Cs loadings on the structure of confined Cs^+ sites and the kinetic regime of ammoxidation over different Cs^+/zeolites under the reaction conditions used in this study. Instead, we have provided Figures S1 and S2 (Supporting Information), which display the influence of Cs loadings (1, 2, 3, 5, and 10 wt %) on the steady-state time-on-stream for the toluene ammoxidation, where all the Cs^+/Y catalysts showed stable performances under the present conditions. The Cs^+/Y catalyst with 2.0 wt % Cs loading was the superior one. The conversion and yield increased with an increase of the catalyst weight up to 0.4 g (for example, the conversion increased from 73.0% to 94.6% with a catalyst increase from 0.2 to 0.4 g, respectively, while keeping a high selectivity of 98.0% (Table 1, Table S3, and Figure 1)), and then the value was saturated, where most of the fed toluene molecules were transformed to benzonitrile (94.6% conversion), thereby bringing almost no supply to the remaining catalyst layer located close to the reactor exit (e.g., 0.1 g in 0.5 g of catalyst) (Figure 1 and Table S3). When the catalyst increased above 0.4 g, the undesirable extra NH_3 oxidation (consumed NH_3/synthesized PhCN) increased (Table S3).

Neither bicomponent reactions of toluene + O_2 (without NH_3) (eq 1), toluene + NH_3 (without O_2) (eq 2), nor NH_3 + O_2 (without toluene) (eq 3) on the Cs^+/Y proceeded as shown in Table 1 as follows.

$$C_6H_5CH_3 + O_2 \rightarrow \text{no oxidation products} \quad (1)$$

$$C_6H_5CH_3 + NH_3 \rightarrow \text{no amination products} \quad (2)$$

$$NH_3 + O_2 \rightarrow \text{no oxidation products} \quad (3)$$

$$C_6H_5CH_3 + 3/2O_2 + NH_3 \rightarrow C_6H_5CN + 3H_2O \text{ with good yield} \quad (4)$$

The toluene ammoxidation (benzonitrile synthesis) proceeded only in the tricomponents reaction (toluene + O_2 + NH_3) (eq 4), indicating the contribution of NH_3 to activation of both toluene C_{sp3}−H and O_2 and no contribution of lattice oxygen atoms of the catalyst to the ammoxidation. Thus, the Cs^+/Y catalyst possesses a unique property: toluene oxidation can be promoted only under the NH_3 coexistence, no toluene amination proceeds, and undesirable NH_3 oxidation with O_2 is suppressed. The activation of both toluene C_{sp3}−H and O_2 by coadsorbed NH_3 and the whole ammoxidation pathway on the

https://doi.org/10.1021/acscatal.1c00946
ACS Catal. 2021, 11, 6698−6708

Cs^+/Y will be discussed in the Coordination-Promoted Concerted Ammoxidation Pathway section. The catalytic performance of Cs^+(2 wt %)/Y did not change during 240 min time-on-stream (Figure S2), and the pore volume (0.990 $cm^3\ g^{-1}$) of the Cs^+(2 wt %)/Y remained unchanged after 240 min of reaction. After 300 min the catalytic conversion at 623 K began to decrease gradually, probably due to coking.[35] However, the pore volume did not reduce significantly. The performance almost recovered by treatment of the 300-min spent catalyst at 673 K in air.

Figure 2 shows the plots of the toluene single-path conversion (%) and benzonitrile selectivity (%) on 0.2 g of the alkali (red mark) and alkaline earth (blue mark) metal ion (2 wt %)/Y catalysts versus the ionic radii of alkali and alkaline earth metal ions to reveal a factor to generate the catalytic performance. In Figure 2 the conversion values for Cs^+/β, Cs^+/Mor, Cs^+/Hydr, and $Cs^+/SiO_2{\cdot}Al_2O_3$ are also plotted for comparison. The conversion increased with an increase of alkali and alkaline earth metal ion radii up to ∼0.14 nm, but the performances of their alkali and alkaline earth metal ions/Y samples were as low as 2.2−17.6% conversions. The Rb^+/Y and Cs^+/Y samples with ion radii larger than ∼0.14 nm, particularly Cs^+/Y (Cs^+ ion diameter = 0.334 nm), showed remarkable conversions with high selectivities (98.1−98.5%). The single Cs^+ sites cannot activate toluene, O_2, and NH_3 when they get adsorbed independently and also in the case of their bicomponents such as toluene + O_2, toluene + NH_3, and NH_3 + O_2 (Table 1). However, when the three reactants (toluene, O_2, and NH_3) coadsorbed together, the trimolecular concerted reaction working closely on the Cs^+ single metal ion site proceeded efficiently, causing toluene C_{sp3}−H activation toward benzonitrile synthesis.

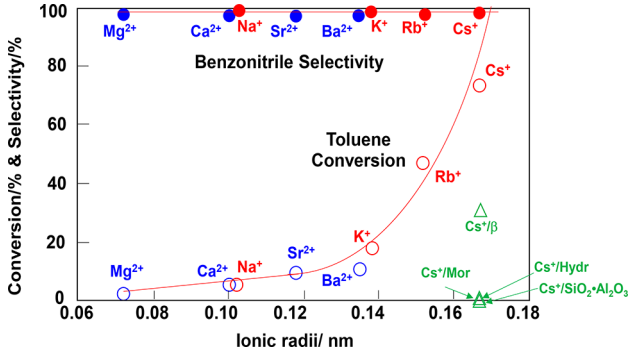

Figure 2. Relation between the catalytic performances (toluene one-path conversion and benzonitrile selectivity) on 0.2 g of the alkali (red mark) and alkaline earth (blue mark) metal ions (2 wt %)/Y catalysts and the ionic radii of alkali and alkaline earth metal ions. The conversion values for Cs^+/β, Cs^+/mordenite (Mor), Cs^+/hydrotalcite (Hydr), and $Cs^+/SiO_2{\cdot}Al_2O_3$ are also plotted for comparison. For reaction conditions, see Table 1.

To gain further insight into the nature of accessible sites in the Cs^+/Y catalyst, the ammoxidation of toluene derivatives with increasing bulkiness was compared with the toluene ammoxidation (Table 2). The Cs^+/Y catalyst showed good performances in achieving the ammoxidation of *o*-, *m*-, and *p*-xylene (81.5−88.8% conversion; 98.0−99.0% selectivity), mesitylene (76.2% conversion; 99.8% selectivity), and *o*-, *m*-, and *p*-chlorotoluene (77.6−91.6% conversion; 94.3−94.6% selectivity). With two bulky alkyl benzene molecules, 1,3,5-tri-*t*-butylbenzene and 1,3,5-tris(2,4,6-trimethylphenyl)benzene, no reactions occurred due to the bulkier sizes than the accessible aperture (0.74 nm) of the Y zeolite with a 3-dimensional network of the open aperture and supercage (1.2 nm),[36] in which Cs^+ ions are confined and bound chemically to the pore surface lattice oxygen atoms (as discussed hereinafter).

3.2. Characterization of Cs^+(2 wt %)/Y by XRD, STEM-EDS, and XAFS. To get an insight into the superiority of Cs^+(2 wt %)/Y, we integrated in situ and ex situ characterization of the Cs^+(2 wt %)/Y catalysts by XRD (Figure S3), STEM-EDS (Figure S4), XPS (Figure 3A), in situ XANES (Figure 3B), in situ EXAFS (Figure 3C), DFT simulations (Figures 4, S5, and S6), and TPD (Figure S7). XRD patterns

Table 2. Catalytic Performances of Cs^+(2 wt %)/Y for Selective Ammoxidation of Substituted Toluenes at 623 K[a]

entry	reactant	reactant conv./%	nitrile selec./%	nitrile syn. rate/μmol s^{-1} g^{-1}_{cat}	NH_3/nitrile
1	*o*-xylene	85.4	98.5[b] (86.6)	0.294	1.0
2	*m*-xylene	81.5	98.0[b] (78.8)	0.275	1.1
3	*p*-xylene	88.8	99.0[b] (92.8)	0.300	0.91
4	mesitylene	76.2	99.8[b] (52.5)	0.228	1.1
5	*o*-chlorotoluene	81.7	94.5	0.288	0.93
6	*m*-chlorotoluene	77.6	94.3	0.274	0.98
7	*p*-chlorotoluene	91.6	94.6	0.322	0.83
8	*o*-nitrotoluene	42.0	96.0	0.148	1.8
9	*m*-nitrotoluene	38.0	98.0	0.134	1.9
10	*p*-nitrotoluene	3.5	99.0	0.012	2.2
11	1,3,5-tri-*tert*-butylbenzene	0		0	
12	1,3,5-Tris(2-methylphenyl)benzene	0		0	

[a]Conv. = conversion; selec. = selectivity. NH_3/nitrile = molar ratios of consumed NH_3 to synthesized nitriles. Performance values were averaged during 30−240 min time-on-stream. Reaction conditions: toluene/O_2/NH_3/He = 0.20/1.0/1.8/4.0 (mL min^{-1}); catal. = 0.4 g; reaction temp = 623 K. [b]Sum of the selectivity (%) of the corresponding mononitrile and dinitrile produced in each entry. The values in the parentheses are the selectivity (%) of the corresponding mononitriles.

https://doi.org/10.1021/acscatal.1c00946
ACS Catal. 2021, 11, 6698−6708

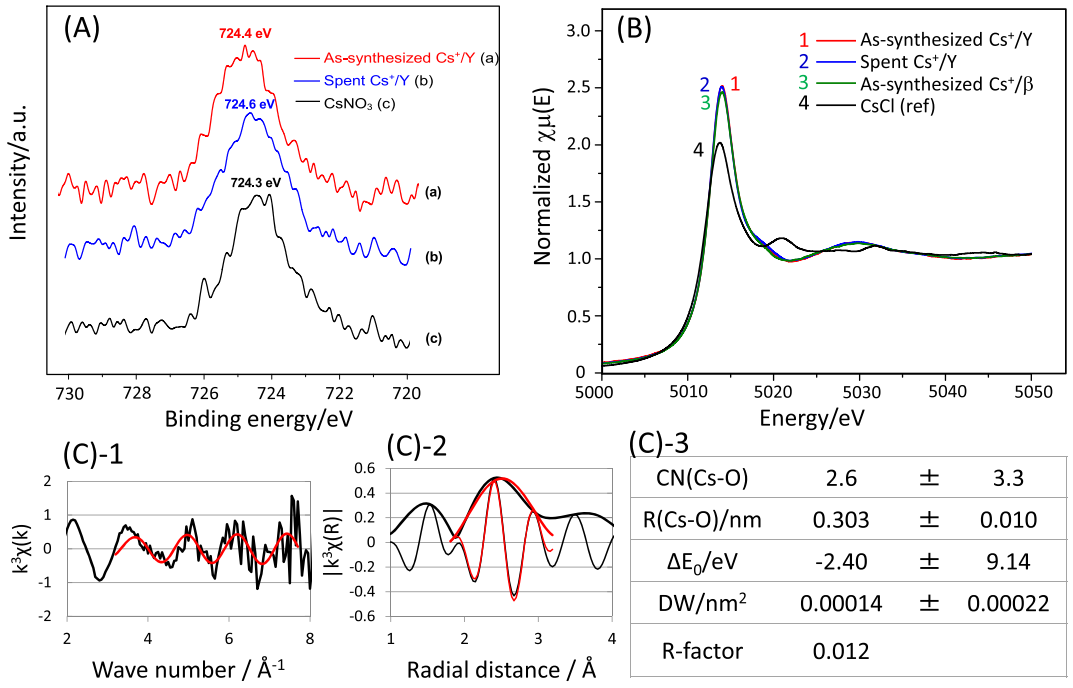

CN(Cs-O)	2.6	±	3.3
R(Cs-O)/nm	0.303	±	0.010
ΔE_0/eV	-2.40	±	9.14
DW/nm^2	0.00014	±	0.00022
R-factor	0.012		

Figure 3. (A) Ex situ XPS Cs $3d_{5/2}$ peaks and binding energies for as-synthesized (fresh) Cs^+(2 wt %)/Y (a; red), spent Cs^+(2 wt %)/Y (b; blue), and $CsNO_3$ (commercial Cs^+ ion salt) (c; black). (B) In situ Cs L_3-edge XANES spectra for as-synthesized (fresh) Cs^+(2 wt %)/Y (1; red), spent Cs^+(2 wt %)/Y (2; blue), and Cs^+(2 wt %)/β (3; green), and ex situ XANES spectrum for CsCl as reference (4; black). (C) In situ Cs L_3-edge EXAFS data and analysis for as-synthesized (fresh) Cs^+(2 wt %)/Y; (C-1) EXAFS oscillation (black, obs; red, fitting); (C-2) EXAFS Fourier transform associated with (C-1) (black, obs; red, fitting; gray, imaginary part; orange, fitting); (C-3) structural parameters for the pretreated Cs/β determined by EXAFS curve-fitting analysis. The EXAFS data were noisy, but the fitting analysis was sufficient for a structural argument.

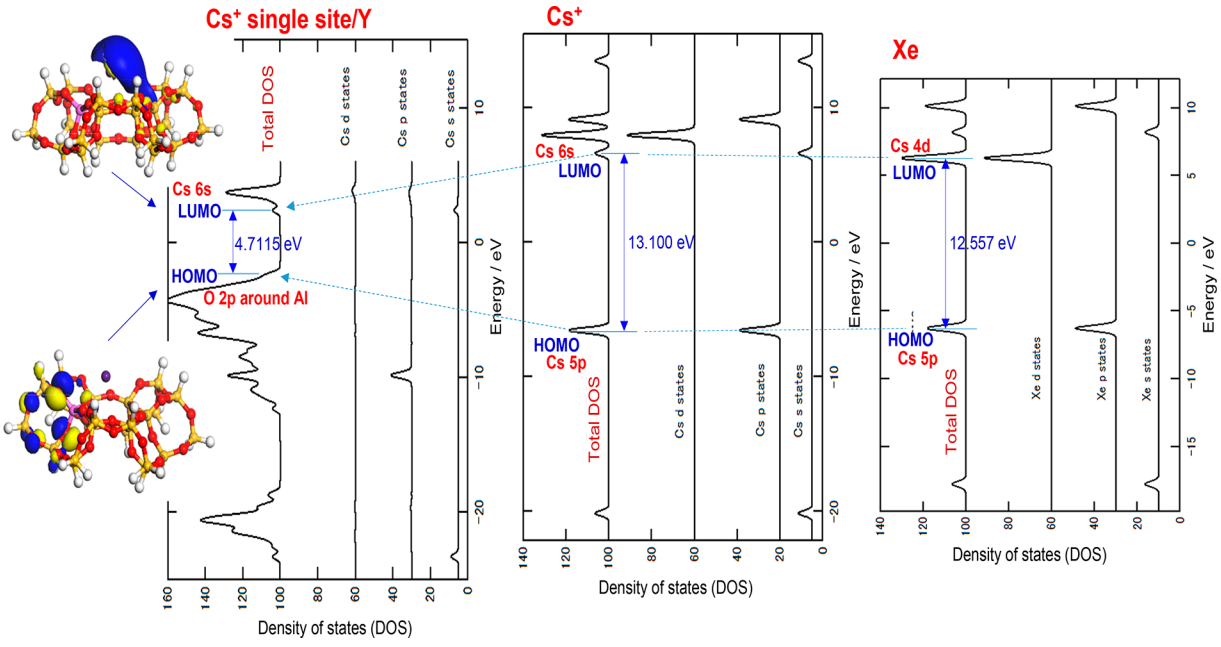

Figure 4. Changes of the energy levels of HOMO and LUMO and the HOMO−LUMO gap by chemical confinement of Cs^+ in Y zeolite pore making Cs−O bonds with pore surface lattice oxygen atoms. Ball−stick model figures for the HOMO and LUMO of Cs^+ single site/Y are also shown.

for the Cs^+/Y samples with 2, 3, 5, and 10 wt % Cs loadings exhibited only typical XRD peaks associated with Y zeolite, and no Cs oxide peaks were observed up to 10 wt % Cs loadings (Figure S3). Bright-field STEM images and element (Si, O, and Cs) EDS maps for Cs^+(2 wt %)/Y revealed no feature except for the Y zeolite lattice (Figure S4). Hence, we measured in situ EXAFS data to obtain information on a local coordination structure around the Cs site. The observed EXAFS data for Cs^+(2.0 wt %)/Y (Figure 3C-1 and C-2) were noisy, but we could do a sufficient fitting analysis of the EXAFS data for a structural argument of single Cs^+ sites. The EXAFS analysis at the Cs L_3-edge for the Cs^+(2 wt %)/Y catalyst in

https://doi.org/10.1021/acscatal.1c00946
ACS Catal. 2021, 11, 6698−6708

Figure 3C revealed only Cs−O bonds at 0.303 (±0.010) nm with an approximate coordination number of 2.6, and no Cs−Cs bonds were observed, which indicates isolated Cs single sites that are chemically bound to three lattice O atoms of the zeolite pore surface. The experimental results were essentially consistent with the theoretically simulated structure around the Cs^+ ion in the pore (Cs−O = 0.315, 0.316, and 0.366 nm), as shown in Figure S5, considering that the local structure determined by EXAFS is an averaged coordination structure at every Cs site involved in the catalyst. The coordination structure of Cs sites in Y zeolite pores (Y zeolite component: SiO_2/Al_2O_3 = 30) resembles that of Cs^+ single sites in β zeolite pores (β zeolite component: SiO_2/Al_2O_3 = 30), while the Cs−O interatomic distances are shorter than 0.335, 0.356, and 0.386 nm, respectively, for Cs^+/β.[1] The Mulliken charges on Cs^+ in Y and β pores were estimated as +0.773 and +0.327, respectively, by DFT, which is due to the shorter and stronger Cs−O bonds in the Cs^+/Y than in the Cs^+/β. It is suggested that the difference in the local structures, Mulliken charges, and pore sizes caused the increased activity of Cs^+/Y compared to Cs^+/β in the catalytic ammoxidation (Table 1). As to the very poor activity of Cs^+/ZSM-5 and Cs^+/MOR, proper local structures around the Cs^+ sites may be obtained for the systems without adsorbed molecules before the ammoxidation catalysis; however, the narrower pores and channel structures (pore diameter of 0.54 × 0.56 nm for ZSM-5 and one-dimensional pore of 0.67 × 0.70 nm in diameter for mordenite), compared to pore diameters of 0.55 × 0.55 nm and 0.76 × 0.64 nm for β and a supercage diameter of 1.2 nm and an open aperture of 0.74 nm for Y, may exert steric constraints for a trimolecular concerted pathway involving large-sized reaction intermediates and transition states (discussed later), resulting in almost no progress of the ammoxidation reaction on Cs^+/ZSM-5 and Cs^+/Mor (Table 1).

Conversely, the Cs^+/β was active for benzene C_{sp2}−H functionalization toward phenol, but the Cs^+/Y was inactive for the phenol synthesis.[1] It is to be noted that the activation of C−H bonds by alkali metal ion single sites is very sensitive to the local structure around the alkali metal ion. Further, the valency of Cs was proved by XPS 3d spectra and in situ XANES (Figure 3A and B). The XPS $3d_{5/2}$ binding energies for the fresh and spent Cs^+/Y catalysts were 724.7 and 724.6 eV, respectively, which are situated in the values for Cs^+ monocations; 724.3 eV for $CsNO_3$; 724.5 eV for CsOH; and 724.8 eV for Cs_2CO_3 on Ag. The white line peak intensity in the in situ Cs L_3-edge XANES spectra for the fresh and spent Cs^+/Y catalysts was much larger than the ex situ XANES spectrum for CsCl with a formal valency of Cs^+. The white line peak intensity in the XANES spectra at the Cs L_3-edge reflects the multielectron photoexcitation feature involving electrons from outer subshells 6s to 4p, and it is also related to Cs valency, which resembles the large white line intensity for Cs^+/β with direct Cs−O bonds.[1] Cs^+ ions with a noble gas electronic structure Coulombically supported on SiO_2 and $SiO_2{\cdot}Al_2O_3$ surfaces were inactive for toluene ammoxidation (Table 1). Inactive Cs^+ ions were transformed to remarkable Cs^+ single sites confined in Y zeolite pores making direct Cs−O bonds with the Y pore surface lattice oxygen atoms (Table 1, Figure 3C, and Figure S5). The density of states (HOMO and LUMO) for Cs^+/Y by DFT calculations using the optimized structural model of Cs^+ single site/Y (Figure S5) is shown in Figure 4 and Figure S6. HOMO and LUMO for free Cs^+ ion are composed of Cs 5p and 6s states, respectively. For the Cs^+ single site chemically confined in the Y zeolite making Cs−O bonds, HOMO and LUMO are composed of O 2p state bonding with the Al atom at the Y pore surface and Cs 6s state on Cs^+, respectively, as shown in Figure 4, where the HOMO−LUMO gap decreased drastically to 4.7115 eV by increasing the HOMO energy and the decreasing LUMO energy (Figure 4 and Figure S6). The LUMO for Cs^+/β with much less activity than Cs^+/Y constitutes O 2p around the Si atom at the β pore surface, and the HOMO−LUMO gap (5.1059 eV) was larger than that for the Cs^+/Y (Figure S6). The energy gap and nature of HOMO and LUMO states are expected to affect the catalytic performance of the Cs^+ single sites for C_{sp3}−H bond activation. This discussion is not limited to the alkali metal ion single sites in Y zeolite pores. For example, Rh/ZSM-5, in which Rh single atoms were attached on ZSM-5 pore surfaces, has been reported to show unique, efficient CH_4 activation toward HCOOH and CH_3COOH at 50 bar, although the origin of the unique catalysis of Rh single atom sites/ZSM-5 has not been investigated in detail.[37]

3.3. Coordination-Promoted Concerted Ammoxidation Pathway. Alkali metal ions do not have the moderate redox property that brings about selective oxidation and ammoxidation, which is suggested by the unchanged XPS and XANES spectra in Figure 3. To estimate the basic and acidic strengths of the Cs^+ single sites/Y catalyst, we conducted temperature-programmed desorption (TPD) of CH_3CN and CO_2 on Cs^+(2 wt %)/Y (Figure S7). The TPD peak for CH_3CN on the Cs^+/Y catalyst was observed at a low temperature around 440 K, and the desorbed CH_3CN amount per Cs^+ after subtracting the amount desorbed from the bare Y zeolite was 66.4% of the Cs^+ quantity. These results indicate a weak Lewis acidity of the Cs^+ single sites in Y zeolite pores, which is a little stronger than the Lewis acidity of the Cs^+ sites in β pores (TPD peak around 360 K). In the TPD of CO_2 on Cs^+(2 wt %)/Y to estimate the basic strength, most of the adsorbed CO_2 desorbed below 323 K and the desorbed amount was negligible (0.1% of Cs^+), indicating a negligible basicity of the Cs^+ single sites in Y pores. Thus, no significant acidity−basicity contribution to the toluene C_{sp3}−H ammoxidation catalysis of Cs^+(2 wt %)/Y is needed in the current study.

Although it is generally agreed that activation of the methyl group is the rate-determining step during the toluene ammoxidation,[3,38,39] the nature of activated species and intermediates is still under debate. We examined the effect of electron-donating and -withdrawing side groups on the aromatic ring (Table 2). The nitrile yields in the ammoxidation of xylene and chlorotoluene varied in the order *p*- > *o*- > *m*-substituents, unlike that reported previously,[40] which might be due to a heterolytic C−H rupture mechanism forming a carbocationic intermediate[41] and involving electronic effects.[42] In the case of nitrotoluene, *p*-nitrotoluene was not converted significantly to *p*-nitrobenzonitrile, whereas *o*-nitrotoluene was transformed to the corresponding nitrile with a similar yield to that for *m*-nitrotoluene (Table 2). Further, the carbocationic intermediate should be accompanied by hydride ion formation, thereby reducing Cs^+ sites partially or fully, which is inconsistent with the in situ Cs L_3-edge XANES spectra that were unchanged during the catalysis (Figure 3B). Hence, the association of the superior catalytic property of Cs^+ single sites to other factors such as the largest size of Cs^+ ion (0.334 nm) among the alkali metal ions and the unaffected Sanderson

https://doi.org/10.1021/acscatal.1c00946
ACS Catal. 2021, 11, 6698−6708

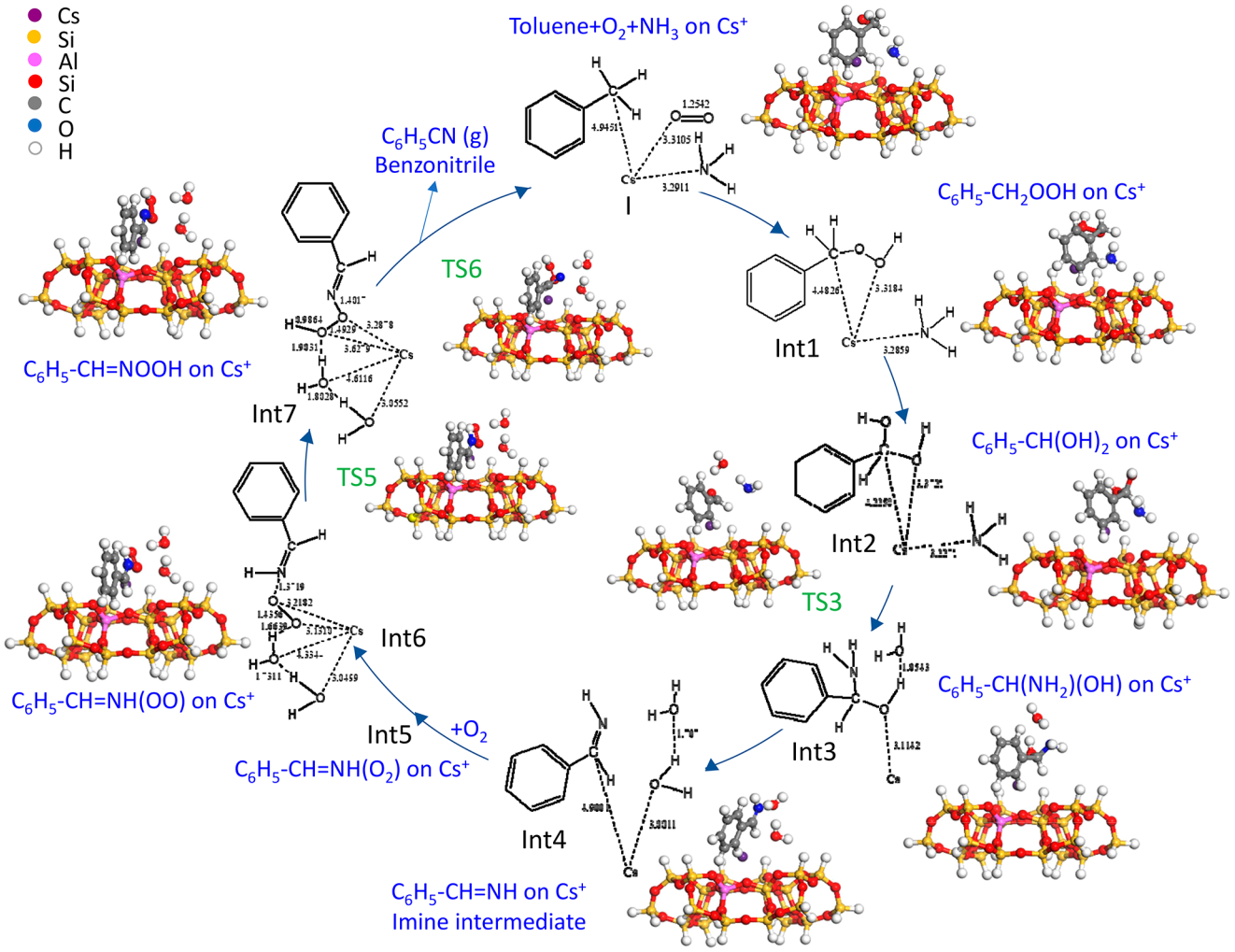

Figure 5. Catalytic cycle (ball−stick model figures) of the ammoxidation of toluene C_{sp3}−H bonds via the inter-coadsorbate reaction pathway without O_2 dissociation and lattice oxygen involvement on a Cs^+ single site in the Y zeolite pore rationalized by DFT calculations involving the reaction intermediates and transition states. For bond distances, see Figures S8 and S9.

electropositivity of the Cs^+ ion is envisioned.[1,43] This hypothesis is supported by the trend of the ion-size effect in the catalytic performance, as shown in Figure 2, and by the methyl cyanation experiment of 3-methylpyridine, where neither aldehyde nor cyanide products were produced because perhaps the electropositivity of Cs^+ was quenched by the lone-pair electrons of 3-methylpyridine. The larger electropositivity and size of the Cs^+ ions stem from the lower polarizabilty or higher softness of the Cs^+ ions, which are further ensconced by their confinement within the zeolite pores.[44] The polarizabilty shuffles with the high electropositivity in the Cs^+/Y, which, in turn, efficiently copes with the energy penalty to overcome the ammoxidation reaction barriers. There was no change in the Cs^+ oxidation state during the catalysis, and thus, the mechanism differs from the traditional redox catalysis (e.g., Mars−van Krevelen mechanism)[45] and also acid−base catalysis involving clearly defined interaction modes.

To shed light on the origin of the selective C_{sp3}−H cyanation performance of the Cs^+ single site/Y catalyst and to understand the ammoxidation mechanism at the molecular level, we performed periodic self-consistent DFT calculations for the reaction pathway. The reaction mechanism, coordination arrangements, and energy profiles involving reaction intermediates and transition states for the toluene ammoxidation on the Cs^+ single site in the Y zeolite pore are shown in Figure 5 (catalytic cycle outline), Figure S8 (reaction pathway), and Figure S9 (detailed mechanism and energy profiles). The significantly large diameter of the Cs^+ ion enables all three reactant molecules ($C_6H_5CH_3$, O_2 and NH_3) to get adsorbed on a Cs^+ single site. It was found that an NH_3 molecule adsorbed/coordinated on a Cs^+ site promotes the toluene C_{sp3}−H activation and O_2 activation accompanied by the C−O bonding on the Cs^+ site to produce hydroperoxy intermediate (Int1 = $C_6H_5CH_2OOH$) via transition state TS1, followed by the formation of *gem*-diol intermediate (Int2 = $C_6H_5CH(OH)_2$), gaining a bond-rearrangement energy of 233.5 kJ mol^{-1} (Figure S9). NH_3 plays an important role in the coadsorption of toluene and O_2 on the Cs^+ single site, where donation from NH_3 to Cs^+ is essential for the interaction between the toluene methyl group and the O_2 molecule on a Cs^+ single site. The adsorption behavior and strength of NH_3 were examined by NH_3 TPD (Figure S10). The NH_3 adsorption behavior at the Cs^+ single sites in the zeolite pores cannot be evidenced from the NH_3 TPD curves, but the NH_3 TPD data are compatible with the trend of Mulliken charges for Cs^+/Y and Cs^+/β by DFT and the fact that NH_3 promotes the toluene ammoxidation more with Cs^+/Y than Cs^+/β. Then, Int2 was transformed to the aminohydroxyto-

https://doi.org/10.1021/acscatal.1c00946
ACS Catal. 2021, 11, 6698−6708

luene intermediate (Int3 = $C_6H_5CH(NH_2)(OH)$) with a C−N bond via a benzaldehyde-type transition state (TS3) that interacts with the coadsorbed NH_3 and H_2O. The hydrogen atom of the C−OH end of Int2 shifts to the other O−H group to form TS3, which consists of distorted benzaldehyde, H_2O, and NH_3. In TS3, the benzaldehyde molecule exhibits a nonplanar conformation, where the plane of the phenyl group and the plane of the carbonyl group form an angle of 41.3°. It is noted that the stable planar benzaldehyde molecule does not appear in the whole reaction pathways. Int3 was dehydrated by the interligand bond rearrangement involving N−H bond scission to form an imine intermediate (Int4 = $C_6H_5CH{=}NH$) via the C−O breaking transition state (TS4), which is stabilized on the Cs^+ single site. The imine N atom interacts with the Cs 6s LUMO as an electron acceptor,[46] resulting in the promotion of the reaction with the second adsorbed O_2 at the N position (Int5 = $C_6H_5CH{=}NH(O_2)$) and Int6 = $C_6H_5CH{=}NH(OO)$), and the interligand rearrangements occur between the two imine H atoms and oxygen successively to produce the $C_6H_5CH{=}NOOH$ intermediate (Int7) via transition state TS5 and benzonitrile $C_6H_5C{\equiv}N$ (F) via transition state TS6 accompanied by H_2O_2 (readily decomposed to H_2O at 623 K). These interligand bond rearrangements are possible with the large-sized (0.334 nm) Cs^+ ion. Finally, the adsorbed benzonitrile (F) desorbs to the gas phase with a desorption energy of 71.0 kJ mol^{-1} in a gas-phase, single-path flow reaction. The rate-determining steps in the whole reaction pathway constitute three C−H and N−H bond-dissociation steps (Int1 → Int2, Int3 → Int4, and Int7 → F) after the first dissociation of toluene C_{sp3}−H bonds (Figure S9). In the catalysis mechanism the Cs^+ single-ion sites confined in the Y zeolite pores provide a trimolecular assembly platform to enable the coordination-promoted concerted ammoxidation pathway without involvements of O_2-dissociated O atom and lattice oxygen.

4. CONCLUSIONS

Industrial vapor-phase ammoxidation reactions have been extensively studied over mixed transition metal oxide catalysts with moderate redox potentials and sufficient M−O bond strengths that bring about active lattice oxygen and oxygen atoms at the catalyst surfaces to promote redox catalysis. However, alkali and alkaline earth metal ions with noble gas electronic structures have been thought to be inactive for selective oxidation processes before our recent report on benzene C_{sp2}−H hydroxylation with N_2O or O_2 toward phenol.[1] The Cs^+ single-ion site/Y catalyst without a beneficial redox property, which was inactive for benzene hydroxylation, showed unprecedented catalysis with high efficiencies toward catalytic cyanation (ammoxidation) of C_{sp3}−H bonds of toluene and its derivatives with NH_3 as test reactions. The molar ratios of [NH_3 consumed]/[nitriles synthesized] were nearly stoichiometric, minimizing undesired extra oxidation of NH_3, which is advantageous industrially. DFT calculations indicated the reduction of the HOMO−LUMO gap and the variation of the HOMO component by the chemical confinement of the Cs^+ single-ion sites in the Y zeolite pores, making Cs−O(lattice) bonds that provided a new trimolecular assembly platform to enable the coordination-promoted concerted pathway that worked closely on the large-sized Cs^+ single site without any significant change of the Cs^+ charge, which is different from the traditional redox catalysis mechanisms (e.g., the Mars−van Krevelen mechanism). At the initial stage of the reaction, NH_3 plays an important role in the coadsorption of toluene and O_2 on Cs^+ single sites, where donation from NH_3 to Cs^+ is essential for the interaction between the toluene methyl group and the O_2 molecule to form a C−O bond on a Cs^+ single site according to the DFT calculations. Then, the neighboring NH_3 molecule joins the ammoxidation reaction, which proceeds successively via several reaction intermediates and transition states with C−N bond, C=N bond, and finally C≡N bond on a large-sized Cs^+ single site confined in the Y zeolite pore. Our synthetic strategy potentially increases the scope of on-demand organic nitrile synthesis by rationally incorporating Cs^+ ions in Y zeolite pores simply by an industrially advantageous facile ion-exchange process.

■ ASSOCIATED CONTENT

Supporting Information

The Supporting Information is available free of charge at https://pubs.acs.org/doi/10.1021/acscatal.1c00946.

Lists of catalytic performance data for Cs^+/Y with different Si/Al ratios, Cs loadings, and catalyst weights; time-on-stream performances (conversion and selectivity) of Cs^+/Y at 623 K; XRD patterns and bright-field STEM-EDS maps; DFT simulations of the optimized structure model of Cs^+/Y and HOMO−LUMO states; TPD curves of CH_3CN and CO_2; DFT computational reaction pathways and energy profiles; and TPD curves of NH_3 (PDF)

■ AUTHOR INFORMATION

Corresponding Authors

Takehiko Sasaki − *Graduate School of Frontier Science, The University of Tokyo, Kashiwa, Chiba 277-8561, Japan;* orcid.org/0000-0001-6190-4087; Email: takehiko@k.u-tokyo.ac.jp

Yasuhiro Iwasawa − *Innovation Research Center for Fuel Cells and Graduate School of Informatics and Engineering, The University of Electro-Communications, Chofu, Tokyo 182 8585, Japan;* orcid.org/0000-0002-5222-5418; Email: iwasawa@pc.uec.ac.jp

Authors

Shankha S. Acharyya − *Innovation Research Center for Fuel Cells and Graduate School of Informatics and Engineering, The University of Electro-Communications, Chofu, Tokyo 182 8585, Japan;* orcid.org/0000-0001-7572-3674

Shilpi Ghosh − *Innovation Research Center for Fuel Cells and Graduate School of Informatics and Engineering, The University of Electro-Communications, Chofu, Tokyo 182 8585, Japan;* orcid.org/0000-0001-6332-0595

Yusuke Yoshida − *Innovation Research Center for Fuel Cells, The University of Electro-Communications, Chofu, Tokyo 182 8585, Japan*

Takuma Kaneko − *Innovation Research Center for Fuel Cells, The University of Electro-Communications, Chofu, Tokyo 182 8585, Japan*

Complete contact information is available at: https://pubs.acs.org/10.1021/acscatal.1c00946

Author Contributions

‖S.S.A., S.G., T.S., and Y.I. contributed equally.

Notes

The authors declare no competing financial interest.

■ ACKNOWLEDGMENTS

The study was supported by Grant-in-Aid for Scientific Research of JSPS/MEXT (16F16078 and 16F16383). S.S.A. and S.G. thank JSPS Postdoctoral Fellowship for foreign researchers. The XAFS measurements were performed with the approval of SPring-8 subject numbers 2017A7808, 2017A7841, 2018A7840, 2018B7840, and 2019A7840.

■ REFERENCES

(1) Ghosh, S.; Acharyya, S. S.; Kaneko, T.; Higashi, K.; Yoshida, Y.; Sasaki, T.; Iwasawa, Y. Confined Single Alkali Metal Ion Platform in a Zeolite Pore for Concerted Benzene C-H Activation to Phenol Catalysis. *ACS Catal.* **2018**, *8*, 11979−11986.

(2) Acharyya, S. S.; Ghosh, S.; Yoshida, Y.; Kaneko, T.; Sasaki, T.; Iwasawa, Y. NH_3 -Driven Benzene C-H Activation with O_2 that Opens a New Way for Selective Phenol Synthesis. *Chem. Rec.* **2019**, *19*, 2069−2081.

(3) Cavalli, P.; Cavani, F.; Manenti, I.; Trifiro, F. Ammoxidation of Toluene to Benzonitrile on Vanadium-Titanium Oxides Catalysts Prepared by Precipitation. The Role of Catalyst Composition. *Ind. Eng. Chem. Res.* **1987**, *26*, 639−647.

(4) Anbarasan, P.; Schareina, T.; Beller, M. Recent Developments and Perspectives in Palladium-Catalyzed Cyanation of Aryl Halides: Synthesis of Benzonitriles. *Chem. Soc. Rev.* **2011**, *40*, 5049−5067.

(5) Sundermeier, M.; Zapf, A.; Mutyala, S.; Baumann, W.; Sans, J.; Weiss, S.; Beller, M. Progress in the Palladium-Catalyzed Cyanation of Aryl Chlorides. *Chem. - Eur. J.* **2003**, *9*, 1828−1836.

(6) Hodgson, H. H. The Sandmeyer Reaction. *Chem. Rev.* **1947**, *40*, 251−277.

(7) Jagadeesh, R. V.; Junge, H.; Beller, M. Green Synthesis of Nitriles using Non-Noble Metal Oxides-Based Nanocatalysts. *Nat. Commun.* **2014**, *5*, 4123.

(8) Yang, J.; Karver, M. R.; Li, W.; Sahu, S.; Devaraj, N. K. Metal-Catalyzed One-Pot Synthesis of Tetrazines Directly from Aliphatic Nitriles and Hydrazine. *Angew. Chem., Int. Ed.* **2012**, *51*, 5222−5225.

(9) Pollak, P.; Romeder, G.; Hagedorn, F.; Gelbke, H. P. *Ullman's Encyclopedia of Industrial Chemistry*; Wiley-VCH Verlag GmbH & Co. KGaA: Weinheim, 2000; DOI: 10.1002/14356007.a17_363.

(10) Wang, L.; Wang, G.; Zhang, J.; Bian, C.; Meng, X.; Xiao, F. S. Controllable Cyanation of Carbon-Hydrogen Bonds by Zeolite Crystals over Manganese Oxide Catalyst. *Nat. Commun.* **2017**, *8*, 15240.

(11) Centi, G.; Marchi, F.; Perathoner, S. Effect of Ammonia Chemisorption on the Surface Reactivity of V-Sb-oxide Catalysts for Propane Ammoxidation. *Appl. Catal., A* **1997**, *149*, 225−244.

(12) Otamiri, J. C.; Andersson, A. Kinetics and Mechanisms in the Ammoxidation of Toluene over a V_2O_5 catalyst. Part 1: Selective Reactions. *Catal. Today* **1988**, *3*, 211−222.

(13) Rapolu, R.; Panja, K. R. Highly selective V-P-O/γ-Al_2O_3 Catalysts in the Ammoxidation of Toluene to Benzonitrile. *J. Chem. Soc., Chem. Commun.* **1993**, 1175−1176.

(14) Sanati, M.; Andersson, A.; Wallenberg, L. R.; Rebenstorf, B. Zirconia-Supported Vanadium Oxide Catalysts for Ammoxidation and Oxidation of Toluene: A Characterization and Activity Study. *Appl. Catal., A* **1993**, *106*, 51−72.

(15) Martin, A.; Berndt, H.; Lücke, B.; Meisel, M. Reaction Pathway of Benzonitrile Formation during Toluene Ammoxidation on Vanadium Phosphate Catalysts. *Top. Catal.* **1996**, *3*, 377−386.

(16) Zhang, Y.; Martin, A.; Berndt, H.; Lücke, B.; Meisel, M. FTIR Investigation of Surface Intermediates Formed during the Ammoxidation of Toluene over Vanadyl Pyrophosphate. *J. Mol. Catal. A: Chem.* **1997**, *118*, 205−214.

(17) Martin, A.; Hannour, F.; Brückner, A.; Lücke, B. Ammoxidation of Toluene on Vanadyl Polyphosphates-$VO(PO_3)_2$, 2. Catalytic Properties. *React. Kinet. Catal. Lett.* **1998**, *63*, 245−251.

(18) Younes, M. K.; Ghorbel, A. Catalytic Nitroxidation of Toluene into Benzonitrile on Chromia-Alumina Aerogel Catalyst. *Appl. Catal., A* **2000**, *197*, 269−277.

(19) Chary, K. V. R.; Reddy, K. R.; Bhaskar, T.; Sagar, G. V. Dispersion and Reactivity of Mo/Nb_2O_5 Catalysts in the Ammoxidation of Toluene to Benzonitrile. *Green Chem.* **2002**, *4*, 206−209.

(20) Rombi, E.; Ferino, I.; Monaci, R.; Picciau, C.; Solinas, V.; Buzzoni, R. Toluene Ammoxidation on α-Fe_2O_3-based Catalysts. *Appl. Catal., A* **2004**, *266*, 73−79.

(21) Teimouri, A.; Najari, B.; Najafi Chermahini, A.; Salavati, H.; Fazel-Najafabadi, M. Characterization and Catalytic Properties of Molybdenum Oxide Catalysts Supported on ZrO_2-γ-Al_2O_3 for Ammoxidation of Toluene. *RSC Adv.* **2014**, *4*, 37679−37686.

(22) Goto, Y.; Shimizu, K.; Kon, K.; Toyao, T.; Murayama, T.; Ueda, W. NH_3-Efficient Ammoxidation of Toluene by Hydrothermally Synthesized Layered Tungsten-Vanadium Complex Metal Oxides. *J. Catal.* **2016**, *344*, 346−353.

(23) Hari Babu, B.; Venkateswara Rao, K. T.; Suh, Y. W.; Sai Prasad, P. S.; Lingaiah, N. One-Step Selective Synthesis of 2-Chlorobenzonitrile from 2-Chlorotoluene via Ammoxidation. *New J. Chem.* **2018**, *42*, 1892−1901.

(24) Li, X.; Sun, L.; Hu, M.; Huang, R.; Huang, C. Hydrothermal Synthesis of Urchin-like W-V-O Nanostructures with Excellent Catalytic Performance. *Inorg. Chem.* **2018**, *57*, 14758−14763.

(25) Centi, G.; Jiru, P.; Trifiro, F. Catalytic Properties of Zeolites in Oxidation and Ammoxidation Reaction. *Stud. Surf. Sci. Catal.* **1989**, *44*, 247−254.

(26) Iwasawa, Y., Asakura, K., Tada, M., Eds. XAFS Techniques for Catalysts. In *Nanomaterials and Surfaces*; Springer: 2016; pp 3−10, 13−50, 299−316.

(27) Ravel, B.; Newville, M. ATHENA, ARTEMIS, HEPHAESTUS: Data Analysis for X-Ray Absorption Spectroscopy using IFEFFIT. *J. Synchrotron Radiat.* **2005**, *12*, 537−541.

(28) Rehr, J. J.; Albers, R. C. Theoretical Approaches to X-Ray Absorption Fine Structure. *Rev. Mod. Phys.* **2000**, *72*, 621−654.

(29) Newville, M.; Ravel, B.; Haskel, D.; Rehr, J. J.; Stern, E. A.; Yacoby, Y. Analysis of Multiple-Scattering XAFS Data Using Theoretical Standards. *Phys. B* **1995**, *208−209*, 154−156.

(30) Delley, B. An All-Electron Numerical method for Solving the Local Density Functional for Polyatomic Molecules. *J. Chem. Phys.* **1990**, *92*, 508−517.

(31) Delley, B. From Molecules to Solids with the DMol3 Approach. *J. Chem. Phys.* **2000**, *113*, 7756−7764.

(32) Perdew, J. P.; Wang, Y. Accurate and Simple Analytic Representation of the Electron-Gas Correlation Energy. *Phys. Rev. B: Condens. Matter Mater. Phys.* **1992**, *45*, 13244−13249.

(33) Halgren, T. A.; Lipscomb, W. N. The Synchronous-Transit Method for Determining Reaction Pathways and Locating Molecular Transition States. *Chem. Phys. Lett.* **1977**, *49*, 225−232.

(34) Bell, S.; Crighton, J. S. Locating Transition States. *J. Chem. Phys.* **1984**, *80*, 2464−2475.

(35) Al-Khattaf, S. Catalytic Transformation of Toluene over a High-Acidity Y-Zeolite Based Catalyst. *Energy Fuels* **2006**, *20*, 946−954.

(36) Verboekend, D.; Nuttens, N.; Locus, R.; Van Aelst, J.; Verolme, P.; Groen, J. C.; Pérez-Ramirez, J.; Sels, B. F. Synthesis, Characterisation, and Catalytic Evaluation of Hierarchical Faujasite Zeolites: Milestones, Challenges, and Future Directions. *Chem. Soc. Rev.* **2016**, *45*, 3331−3352.

(37) Tang, Y.; Li, Y.; Fung, V.; Jiang, D.; Huang, W.; Zhang, S.; Iwasawa, Y.; Sakata, T.; Nguyen, L.; Zhang, X.; Frenkel, A. I.; Tao, F. Single Rhodium Atoms Anchored in Micropores for Efficient Transformation of Methane under Mild Conditions. *Nat. Commun.* **2018**, *9*, 1231.

(38) Lücke, B.; Narayana, K. V.; Martin, A.; Jähnisch, K. Oxidation and Ammoxidation of Aromatics. *Adv. Synth. Catal.* **2004**, *346*, 1407−1424.

(39) Ghosh, S.; Acharyya, S. S.; Tripathi, D.; Bal, R. Preparation of Silver-Tungsten Nanostructure Materials for Selective Oxidation of

Toluene to Benzaldehyde with Hydrogen Peroxide. *J. Mater. Chem. A* **2014**, *2*, 15726−15733.
(40) Busca, G.; Cavani, F.; Trifirò, F. Oxidation and Ammoxidation of Toluene over Vanadium-Titanium Oxide Catalysts: A Fourier Transform Infrared and Flow Reactor Study. *J. Catal.* **1987**, *106*, 471−482.
(41) Lücke, B.; Martin, A. *Catalysis of Organic Reactions*; Scaros, M. G., Prunier, M. L., Eds.; Marcel Dekker, Inc.: 1994; pp 479−482.
(42) Mirth, G.; Cejka, J.; Lercher, J. Transport and Isomerization of Xylenes over HZSM-5 Zeolites. *J. Catal.* **1993**, *139*, 24−33.
(43) Keller, T. C.; Desai, K.; Mitchell, S.; Pérez-Ramírez, J. Design of Base Zeolite Catalysts by Alkali-Metal Grafting in Alcoholic Media. *ACS Catal.* **2015**, *5*, 5388−5396.
(44) Boronat, M.; Corma, A. What Is Measured When Measuring Acidity in Zeolites with Probe Molecules? *ACS Catal.* **2019**, *9*, 1539−1548.
(45) Mars, P.; van Krevelen, D. W. Oxidations Carried out by Means of Vanadium Oxide Catalysts. *Chem. Eng. Sci.* **1954**, *3*, 41−59.
(46) Zachariasse, K. A.; Grobys, M.; von der Haar, T.; Hebecker, A.; Il'ichev, Y. V.; Morawski, O.; Ruckert, I.; Kuhnle, W. Photo-Induced Intramolecular Charge Transfer and Internal Conversion in Molecules with a Small Energy Gap Between S1 and S2. Dynamics and Structure. *J. Photochem. Photobiol., A* **1997**, *105*, 373−383.

https://doi.org/10.1021/acscatal.1c00946
ACS Catal. 2021, 11, 6698−6708